Contents lists available at ScienceDirect

Soil Dynamics and Earthquake Engineering

journal homepage: www.elsevier.com/locate/soildyn

Random vibration analysis of long-span structures subjected to spatially varying ground motions

Y.H. Zhang [a,*], Q.S. Li [b], J.H. Lin [a], F.W. Williams [c]

[a] State Key Laboratory of Structural Analysis for Industrial Equipment, Dalian University of Technology, Dalian 116023, China
[b] Department of Building and Construction, City University of Hong Kong, Kowloon, Hong Kong
[c] Cardiff School of Engineering, Cardiff University, Cardiff CF24 3AA, UK

ARTICLE INFO

Article history:
Received 3 March 2008
Received in revised form
23 April 2009
Accepted 24 June 2009

Keywords:
Random vibration
Earthquake
Wave passage effect
Incoherence effect
Site–response effect

ABSTRACT

On the basis of the pseudo-excitation method (PEM), a random vibration methodology is formulated for the seismic analysis of multi-supported structures subjected to spatially varying ground motions. The ground motion spatial variability consists of the wave passage, incoherence and site–response effects. Advantages of this method are that less computation effort is required and that the cross-correlations both between normal modes and between excitations are automatically included. Random seismic responses of a realistic long-span bridge due to the wave passage, incoherence and site–response effects are extensively investigated. It is shown that all these effects have significant influence on the seismic response of the structure.

1. Introduction

Seismic analysis of long-span structures subjected to spatially varying ground motions has been a fundamental problem of interest for over two decades. Interest in this problem stems from earthquake engineering for the complex nature of the earth's crust, which causes earthquake motions to vary along the length of structures, coupled with the increasing application of long-span structures. The variations in the ground motion arise mainly from three sources: the "wave passage effect" due to the difference in the arrival times of waves at support points; the "incoherence effect" due to reflections and refractions of seismic waves through the soil during their propagation; and the "site-response effect" due to the differences in local soil conditions at the support points [1,2]. Long-span structures are generally important facilities, e.g. long-span bridges, gymnasiums, dams, or nuclear power plants. Therefore, their aseismatic capabilities are highly relevant to public safety and so in the last 20 years much research has gone into establishing practical seismic analysis and design methods for them [3–32].

Lee and Penzien [3] developed a stochastic method for seismic analysis of structures and piping systems subjected to multiple support excitations in both the time and frequency domains. Lin et al. [4] simplified a surface-mounted pipeline as an infinitely long Bernoulli–Euler beam attached to evenly spaced ground supports, and solved its random seismic responses. Perotti [5] investigated the non-stationary responses of multiple-supported structures. Loh and Lee [6] studied the aseismic displacement of multi-supported bridge to multiple seismic excitations. Yamamura and Tanaka [7] developed response spectrum and time–history methods to evaluate the response of MDF systems subjected to multiple-support seismic excitations, with the support motions grouped into independent subgroups with perfect correlation between the members of each subgroup. Deodatis et al. [8] discussed the effect of spatial variability, including variable soil conditions, on the response of bridges using fragility analyses. Zerva [9] analyzed two- and three-span beams of various lengths (short, moderate and long) subjected to input motions that exhibit loss of coherence only, with various degrees of correlation, and compared the response to the one induced by fully correlated motions. The results indicates that fully correlated motions may produce higher or lower response than partially correlated motions, depending on the dynamic characteristics of the structure. Zerva further investigated the effects of both loss of coherence and phase difference between the motions at the supports [10] and isolated the contribution of the different coherency models to the quasi-static and dynamic response of linear, generic models of lifelines [9–12]. It was shown [12] that the root-mean-square (rms) quasi-static response of lifelines is proportional to the rms differential displacement

* Corresponding author. Tel.: +86 411 84706337; fax: +86 411 84708400.
E-mail address: zhangyh@dlut.edu.cn (Y.H. Zhang).

between the supports, and the rms contribution to the excitation of individual modes is proportional to the differential response spectrum. Berrah and Kausel [13] proposed a modified spectrum method for the design of extended structures which considers the spatial variability effect arising from the incoherence. Nazmy and Abdel-Ghaffar [14] studied the seismic responses of cable-stayed bridges considering the seismic-wave traveling effect and accounted for time delay and phase difference by using the time–history method. Der Kiureghian et al. [15] developed a response spectrum method considering the effects of wave passage, incoherence and site–response. Heredia-Zavoni and Vanmarcke [16] developed a random vibration method for the seismic–response analysis of linear multi-support structural systems, which reduces the response evaluation to that of a series of linear one-degree systems in a way that fully accounts for the multiple-support input and the space–time correlation structure of the ground motion. Harichandran et al. [17–20] proposed a random vibration algorithm to reduce the cost of large-scale stationary and transient random vibration analysis of structures excited by multiple partially correlated nodal and/or base excitations, presented stationary and transient response analyses of the Golden Gate suspension bridge, and the New River Gorge and Cold Spring Canyon deck arch bridges. Recently, Tubino et al. [21] provided mathematical and physical interpretations of the effects of partial correlation of the seismic ground motion on the response of multi-supported multi-DOF systems by introducing suitable equivalent spectra and by representing the seismic ground motion by the proper orthogonal decomposition. Allam and Datta [22,23] used frequency domain spectral method and response spectrum method to estimate the seismic responses of cable-stayed bridges subjected to patially correlated stationary random ground motion. Dumanoglu and Soyluk [25–27] investigated the relative importance of ground motion variability effects on the dynamic behavior of plane models of cable-stayed and suspension bridges. Lupoi et al. [28] investigated the relevance of the phenomenon of spatial variability of seismic ground motion on the performance of a number of bridges having quite different distributions of stiffness properties. All these studies have made significant contributions to the seismic analysis of long-span structures.

Lin et al. [29–31] proposed an efficient pseudo-excitation method (PEM) to compute the stationary and non-stationary seismic responses of multi-support structures, for which the wave passage and incoherence effects are included. Zhang et al. [32] used PEM to investigate seimic random responses of a suspension bridge due to the wave passage effect. In the present paper, PEM is extended to investigate the combined influence of the spatial effects of the site–response effect as well as the wave passage and incoherence effects of ground motion on the seismic responses of long-span structures. In order to focus attention on the spatial variation effects, transient dynamic phenomena that may prejudice or compromise a simple interpretation of the most relevant physical and analytical aspects are ignored and the ground motion is modeled as a stationary multivariate, one-dimensional random process. Firstly, the PSD matrix of the ground motions are established based on the coherency model proposed by Der Kiureghian [2]. It accounts for the wave passage, incoherence and site–response effects. It is then decomposed into the product of a matrix and its transpose, and a series of harmonic loads, i.e. so-called pseudo-excitations, are constructed. The PSDs of random seismic responses are then obtained by solving a series of harmonic dynamic equations by using the mode superposition method. The cross-correlations both between normal modes and between excitations are automatically included in the computation. A realistic long-span suspension bridge is analyzed to enable the influence of the wave passage effect, the incoherence effect and the site–response effect to be further discussed.

2. Spatially varying ground motion model

The seismic ground motion is assumed to be a normal stationary random process. If a structure has N supports, their ground accelerations $\ddot{u}_i\,(i=1,2,\ldots,N)$ along the earthquake wave traveling direction can be written as the N-dimensional vector:

$$\ddot{\boldsymbol{u}}_b(t)=\{\,\ddot{u}_1(t)\quad \ddot{u}_2(t)\quad \cdots\quad \ddot{u}_N(t)\,\}^{\mathrm{T}} \tag{1}$$

where superscript T denotes transpose. The spatial variability of the ground motion is characterized by the cross-power spectral density function in the frequency domain. For ground accelerations $\ddot{u}_k(t)$ and $\ddot{u}_l(t)$ at the kth and lth supports, this function can be written as follows:

$$S_{kl}(\omega)=\gamma_{kl}(\omega)\sqrt{S_{kk}(\omega)S_{ll}(\omega)} \tag{2}$$

where ω is the circular frequency; $S_{kk}(\omega)$, $S_{ll}(\omega)$ and $S_{kl}(\omega)$ are the auto-power spectral density functions of the accelerations at the kth and lth supports and their cross-power spectral density function, respectively; and $\gamma_{kl}(\omega)$ is the coherency function of the accelerations at the kth and lth supports, which can be expressed as follows [2]:

$$\gamma_{kl}(\omega)=\gamma_{kl}^{(i)}(\omega)\gamma_{kl}^{(w)}(\omega)\gamma_{kl}^{(s)}(\omega) \tag{3}$$

in which $\gamma_{kl}^{(i)}(\omega)$ characterizes the real-valued incoherence effect, $\gamma_{kl}^{(w)}(\omega)$ indicates the complex-valued wave passage effect and $\gamma_{kl}^{(s)}(\omega)$ defines the complex-valued site–response effect.

Several models have been proposed for the incoherence effect due to reflections and refractions of waves through the soil during their propagation [2,33–35]. For example, Der Kiureghian [2] proposed the mathematic model:

$$\gamma_{kl}^{(i)}(\omega)=\cos\left[\beta(d_{kl},\omega)\right]\exp[-\tfrac{1}{2}\alpha^2(d_{kl},\omega)] \tag{4}$$

in which d_{kl} is the horizontal distance between the two supports and the angles α and β are functions of d_{kl} and ω.

The wave passage effect resulting from the difference in the arrival times of waves at support points is defined as follows [2]:

$$\gamma_{kl}^{(w)}=\exp[\mathrm{i}(\theta_{kl}^{(w)}(\omega)]=\exp\left[-\frac{\mathrm{i}\omega d_{kl}^{L}}{v_{\mathrm{app}}}\right] \tag{5}$$

here d_{kl}^{L} is the projection of d_{kl} in the earthquake propagation direction and, v_{app} is the apparent velocity of the seismic waves, which is usually taken as a constant in practical computations. Suppose that the wave front reaches the origin of the coordinate system, i.e. the reference point, at $T=0$, and then reaches the N supports of the structure at times T_1, T_2, …, T_N, respectively. Without losing generality, we can assume $T_l \geqslant T_k$ and hence

$$\frac{d_{kl}^{L}}{v_{\mathrm{app}}}=T_l-T_k \tag{6}$$

and

$$\gamma_{kl}^{(w)}=\exp[\mathrm{i}\omega(T_k-T_l)] \tag{7}$$

The site–response effect due to the differences in the local soil conditions is obtained as follows [2]:

$$\gamma_{kl}^{(s)}(\omega)=\exp[\mathrm{i}\theta_{kl}^{(s)}(\omega)] \tag{8}$$

and the phase angle is given by

$$\theta_{kl}^{(s)}(\omega)=\theta_{k}^{(s)}(\omega)-\theta_{l}^{(s)}(\omega) \tag{9}$$

in which

$$\theta_k^{(s)}(\omega) = \tan^{-1}\frac{\mathrm{Im}(H_k(\omega))}{\mathrm{Re}(H_k(\omega))} = \tan^{-1}\frac{-2\xi_k\omega_k\omega^3}{\omega_k^2(\omega_k^2-\omega^2)+4\xi_k^2\omega_k^2\omega^2} \quad (10)$$

ω_k and ξ_k are the resonant frequency and damping ratio of the soil layer and Im(♯) and Re(♯) denote the real and imaginary parts of ♯, respectively.

Therefore, the PSD matrix of the ground acceleration vector $\ddot{\boldsymbol{u}}_b(t)$ for the N supports has the form:

$$\boldsymbol{S}_{\ddot{\boldsymbol{u}}_b\ddot{\boldsymbol{u}}_b}(\omega) = \begin{bmatrix} \gamma_{11}^{(i)}S_{11} & \gamma_{12}^{(i)}e^{i(\theta_1^{(s)}-\theta_2^{(s)})}e^{i\omega(T_1-T_2)}\sqrt{S_{11}S_{22}} & \cdots & \gamma_{1N}^{(i)}e^{i(\theta_1^{(s)}-\theta_N^{(s)})}e^{i\omega(T_1-T_N)}\sqrt{S_{11}S_{NN}} \\ \gamma_{21}^{(i)}e^{i(\theta_2^{(s)}-\theta_1^{(s)})}e^{i\omega(T_2-T_1)}\sqrt{S_{22}S_{11}} & \gamma_{22}^{(i)}S_{22} & \cdots & \gamma_{2N}^{(i)}e^{i(\theta_2^{(s)}-\theta_N^{(s)})}e^{i\omega(T_2-T_N)}\sqrt{S_{22}S_{NN}} \\ \vdots & \vdots & \ddots & \vdots \\ \gamma_{N1}^{(i)}e^{i(\theta_N^{(s)}-\theta_1^{(s)})}e^{i\omega(T_N-T_1)}\sqrt{S_{NN}S_{11}} & \gamma_{N2}^{(i)}e^{i(\theta_N^{(s)}-\theta_2^{(s)})}e^{i\omega(T_N-T_2)}\sqrt{S_{NN}S_{22}} & \cdots & \gamma_{NN}^{(i)}S_{NN} \end{bmatrix} \quad (11)$$

in which S_{kk} ($k = 1, 2, \ldots, N$) stands for $S_{kk}(\omega)$.

Obviously, this can be decomposed as follows:

$$\boldsymbol{S}_{\ddot{\boldsymbol{u}}_b\ddot{\boldsymbol{u}}_b}(\omega) = \boldsymbol{B}^*\boldsymbol{D}\boldsymbol{\Gamma}\boldsymbol{D}\boldsymbol{B} \quad (12)$$

in which "*" denotes complex conjugate, and

$$\boldsymbol{B} = \mathrm{diag}\left[\, e^{-i(\omega T_1+\theta_1^{(s)})} \quad e^{-i(\omega T_2+\theta_2^{(s)})} \quad \cdots \quad e^{-i(\omega T_N+\theta_N^{(s)})} \,\right] \quad (13)$$

$$\boldsymbol{D} = \mathrm{diag}\left[\, \sqrt{S_{11}} \quad \sqrt{S_{22}} \quad \cdots \quad \sqrt{S_{NN}} \,\right] \quad (14)$$

$$\boldsymbol{\Gamma} = \begin{bmatrix} \gamma_{11}^{(i)} & \gamma_{12}^{(i)} & \cdots & \gamma_{1N}^{(i)} \\ \gamma_{21}^{(i)} & \gamma_{22}^{(i)} & \cdots & \gamma_{2N}^{(i)} \\ \vdots & \vdots & \ddots & \vdots \\ \gamma_{N1}^{(i)} & \gamma_{N2}^{(i)} & \cdots & \gamma_{NN}^{(i)} \end{bmatrix} \quad (15)$$

In general $\boldsymbol{S}_{\ddot{\boldsymbol{u}}_b\ddot{\boldsymbol{u}}_b}(\omega)$ in Eq. (12) is a positive definite Hermitian matrix, while $\boldsymbol{\Gamma}$ is a positive definite real symmetric matrix, which can be decomposed into the product of a real lower triangle matrix $\boldsymbol{Q}$ and its transpose, i.e.:

$$\boldsymbol{\Gamma} = \boldsymbol{Q}\boldsymbol{Q}^{\mathrm{T}} \quad (16)$$

Thus, Eq. (12) can be written as follows:

$$\boldsymbol{S}_{\ddot{\boldsymbol{u}}_b\ddot{\boldsymbol{u}}_b}(\omega) = \boldsymbol{P}^*\boldsymbol{P}^{\mathrm{T}} \quad (17)$$

in which

$$\boldsymbol{P} = \boldsymbol{B}\boldsymbol{D}\boldsymbol{Q} \quad (18)$$

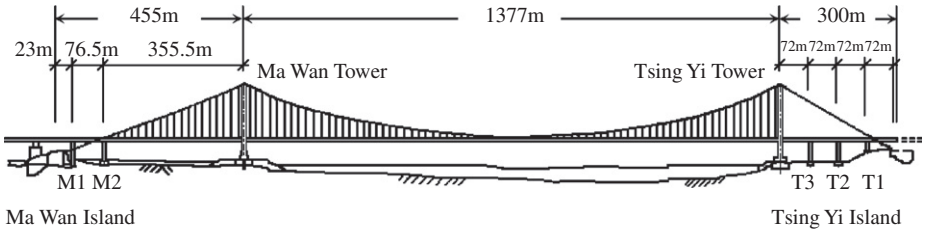

Fig. 1. The Hong Kong Tsing-Ma bridge.

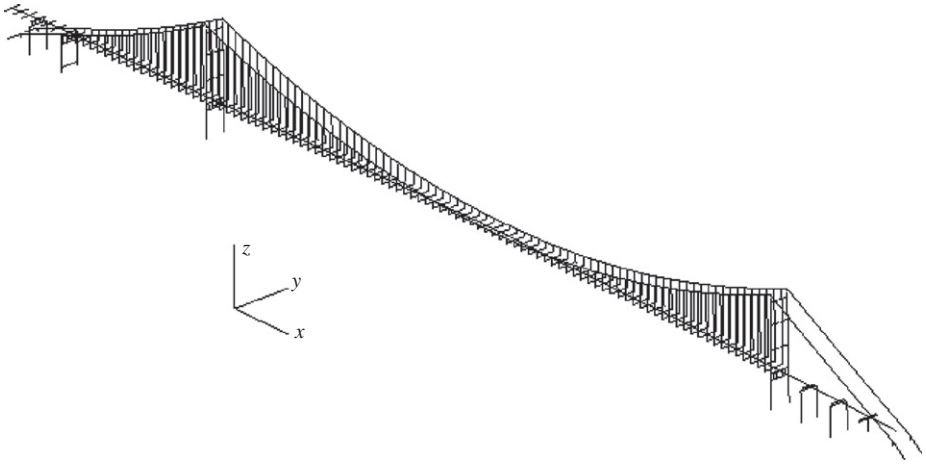

Fig. 2. Finite element model of the Tsing-Ma bridge.

3. Pseudo-excitation method with spatially varying ground motions

The coupled equations of motion of a linear, multi-degree-of-freedom, structural system with N supports subjected to spatially varying ground motions can be written as follows:

$$\begin{bmatrix} \boldsymbol{M} & \boldsymbol{M}_C \\ \boldsymbol{M}_C^T & \boldsymbol{M}_G \end{bmatrix} \begin{Bmatrix} \ddot{\boldsymbol{u}} \\ \ddot{\boldsymbol{u}}_G \end{Bmatrix} + \begin{bmatrix} \boldsymbol{C} & \boldsymbol{C}_C \\ \boldsymbol{C}_C^T & \boldsymbol{C}_G \end{bmatrix} \begin{Bmatrix} \dot{\boldsymbol{u}} \\ \dot{\boldsymbol{u}}_G \end{Bmatrix} + \begin{bmatrix} \boldsymbol{K} & \boldsymbol{K}_C \\ \boldsymbol{K}_C^T & \boldsymbol{K}_G \end{bmatrix} \begin{Bmatrix} \boldsymbol{u} \\ \boldsymbol{u}_G \end{Bmatrix} = \begin{Bmatrix} 0 \\ \boldsymbol{F}_G \end{Bmatrix} \tag{19}$$

in which $\boldsymbol{u}_G$ is the m-dimensional vector of enforced support displacement components, with all three translations and no rotational components considered for each support so that $m = 3N$; $\boldsymbol{u}$ is an n-dimensional vector containing all nodal displacements except those at the supports; $\boldsymbol{F}_G$ represents the enforced forces at all supports; the $n \times n$ matrices $\boldsymbol{M}$, $\boldsymbol{C}$ and $\boldsymbol{K}$ are respectively the mass, damping and stiffness matrices associated with $\boldsymbol{u}$; the $m \times m$ matrices $\boldsymbol{M}_G$, $\boldsymbol{C}_G$ and $\boldsymbol{K}_G$ are the mass, damping and stiffness matrices associated with $\boldsymbol{u}_G$ and; $\boldsymbol{M}_C$, $\boldsymbol{C}_C$ and $\boldsymbol{K}_C$ are the $n \times m$ coupling matrices shown. Note that when the lumped mass matrix approximation is adopted, $\boldsymbol{M}_C$ is null. In order to solve Eq. (19), $\boldsymbol{u}$ is usually decomposed into the two parts:

$$\boldsymbol{u} = \boldsymbol{u}^s + \boldsymbol{u}^d \tag{20}$$

where $\boldsymbol{u}^s$ and $\boldsymbol{u}^d$ are, respectively, the quasi-static and dynamic displacement vectors, which satisfy the equations [15,36]:

$$\boldsymbol{u}^s = -\boldsymbol{K}^{-1}\boldsymbol{K}_C\boldsymbol{u}_G \equiv \boldsymbol{R}\boldsymbol{u}_G \tag{21}$$

$$\boldsymbol{M}\ddot{\boldsymbol{u}}^d + \boldsymbol{C}\dot{\boldsymbol{u}}^d + \boldsymbol{K}\boldsymbol{u}^d = -(\boldsymbol{M}\boldsymbol{R} + \boldsymbol{M}_C)\ddot{\boldsymbol{u}}_G \tag{22}$$

Assume that xyz is a right-hand coordinate system for which both the x- and y-axes lie in the horizontal plane. The anti-clockwise angle between the x-axis and the horizontal traveling direction of earthquake wave is β. Thus, the displacement components along the coordinate axes, $\boldsymbol{u}_G$, can be expressed in terms of the components parallel or normal to the wave traveling direction, $\boldsymbol{u}_b$, as:

$$\boldsymbol{u}_G = \boldsymbol{E}_{mN}\boldsymbol{u}_b \tag{23}$$

in which $\boldsymbol{E}_{mN}$ is an $m \times N$ block-diagonal matrix.

$$\boldsymbol{E}_{mN} = \mathrm{diag}[\,\boldsymbol{E}_1 \quad \boldsymbol{E}_2 \quad \cdots \quad \boldsymbol{E}_N\,] \tag{24}$$

Because only the three translations of each support are considered, each sub-matrix $\boldsymbol{E}_i$ becomes $[\cos\beta \quad \sin\beta \quad 0]^T$, $[-\sin\beta \quad \cos\beta \quad 0]^T$ and $[0 \quad 0 \quad 1]^T$ for the P, SH and SV waves, respectively [31].

Using Eq. (23), Eqs. (21) and (22) can be rewritten as follows:

$$\boldsymbol{u}^s = -\boldsymbol{K}^{-1}\boldsymbol{K}_C\boldsymbol{u}_G \equiv \boldsymbol{R}\boldsymbol{E}_{mN}\boldsymbol{u}_b \tag{25}$$

$$\boldsymbol{M}\ddot{\boldsymbol{u}}^d + \boldsymbol{C}\dot{\boldsymbol{u}}^d + \boldsymbol{K}\boldsymbol{u}^d = -(\boldsymbol{M}\boldsymbol{R} + \boldsymbol{M}_C)\boldsymbol{E}_{mN}\ddot{\boldsymbol{u}}_b \tag{26}$$

Table 1
Selected angular natural frequencies of the Tsing-Ma bridge (rad/s)

Mode	1	2	3	4	5	6	7
Frequency	0.426	0.732	0.863	0.988	1.190	1.322	1.448
Mode	8	9	10	11	12	13	14
Frequency	1.460	1.507	1.538	1.704	1.766	1.828	1.848
Mode	15	16	20	30	40	50	60
Frequency	1.951	2.039	2.312	2.988	3.763	4.507	5.348
Mode	70	80	90	100	110	120	130
Frequency	5.987	6.794	7.727	8.251	9.142	10.032	10.659
Mode	140	150	160	170	180	190	200
Frequency	11.174	12.404	12.967	13.483	14.353	14.962	15.456

Table 2
Power spectral density parameters for firm, medium and soft soil conditions

Soil type	ω_g (rad/s)	ξ_g	ω_f (rad/s)	ξ_g	S_0 (m^2/s^3)
Firm	15.0	0.6	1.5	0.6	0.00177
Medium	10.0	0.4	1.0	0.6	0.00263
Soft	5.0	0.2	0.5	0.6	0.00369

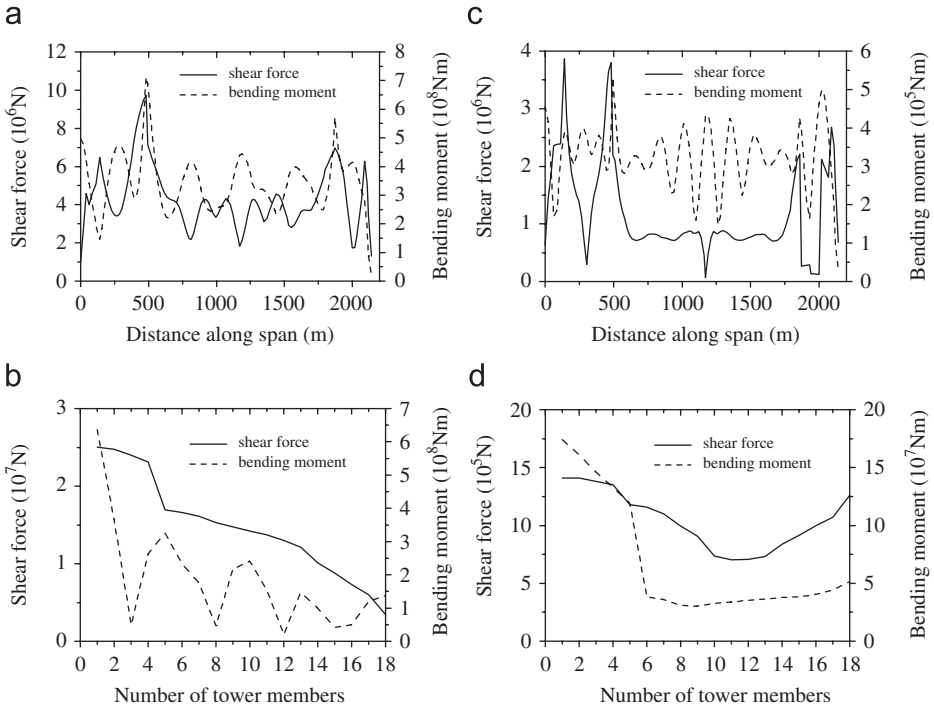

Fig. 3. Shear forces and bending moments under uniform support motions.

Let any response quantity of interest be denoted by $\boldsymbol{z}(t)$, i.e. $\boldsymbol{z}(t)$, could be a nodal displacement vector, an internal force vector, a stress vector or a strain vector. Then for a linear system $\boldsymbol{z}(t)$ can be expressed as follows:

$$z(t) = \boldsymbol{T}^{\mathrm{T}}\boldsymbol{u}(t) + \boldsymbol{T}_{\mathrm{G}}^{\mathrm{T}}\boldsymbol{u}_{\mathrm{G}}(t) \tag{27}$$

where $\boldsymbol{T}^{\mathrm{T}}$ and $\boldsymbol{T}_{\mathrm{G}}^{\mathrm{T}}$ are transfer matrices, which usually depend on the geometry and stiffness properties of the structural system. The dynamic displacement vector can then be written in the convolution integral form as follows:

$$\boldsymbol{u}^{\mathrm{d}}(t) = -\int_{-\infty}^{\infty} \boldsymbol{h}(\tau)(\boldsymbol{MR} + \boldsymbol{M}_{\mathrm{C}})\boldsymbol{E}_{mN}\ddot{\boldsymbol{u}}_b(t-\tau)\,\mathrm{d}\tau \tag{28}$$

in which $\boldsymbol{h}(t)$ is the impulse response function matrix. Hence, using Eqs. (23), (25) and (28), Eq. (27) becomes:

$$z(t) = -\boldsymbol{T}^{\mathrm{T}}\int_{-\infty}^{\infty} \boldsymbol{h}(\tau)\boldsymbol{A}\ddot{\boldsymbol{u}}_b(t-\tau)\,\mathrm{d}\tau + \boldsymbol{G}\boldsymbol{u}_b(t) \tag{29}$$

where

$$\boldsymbol{A} = (\boldsymbol{MR} + \boldsymbol{M}_{\mathrm{C}})\boldsymbol{E}_{mN}, \quad \boldsymbol{G} = \boldsymbol{T}^{\mathrm{T}}\boldsymbol{R}\boldsymbol{E}_{mN} + \boldsymbol{T}_{\mathrm{G}}^{\mathrm{T}}\boldsymbol{E}_{mN}. \tag{30}$$

Then the power spectrum density matrix of $\boldsymbol{z}(t)$ can be obtained as follows:

$$\begin{aligned}\boldsymbol{S}_{zz}(\omega) = {} & \boldsymbol{T}^{\mathrm{T}}\boldsymbol{H}^{*}(\omega)\boldsymbol{A}\boldsymbol{S}_{\ddot{u}_b\ddot{u}_b}(\omega)\boldsymbol{A}^{\mathrm{T}}\boldsymbol{H}^{\mathrm{T}}(\omega)\boldsymbol{T} + \frac{1}{\omega^4}\boldsymbol{G}\boldsymbol{S}_{\ddot{u}_b\ddot{u}_b}(\omega)\boldsymbol{G}^{\mathrm{T}} \\ & + \frac{1}{\omega^2}\boldsymbol{T}^{\mathrm{T}}\boldsymbol{H}^{*}(\omega)\boldsymbol{A}\boldsymbol{S}_{\ddot{u}_b\ddot{u}_b}(\omega)\boldsymbol{G}^{\mathrm{T}} \\ & + \frac{1}{\omega^2}\boldsymbol{G}\boldsymbol{S}_{\ddot{u}_b\ddot{u}_b}(\omega)\boldsymbol{A}^{\mathrm{T}}\boldsymbol{H}^{\mathrm{T}}(\omega)\boldsymbol{T}\end{aligned} \tag{31}$$

in which $\boldsymbol{H}(\omega)$ is the frequency response function matrix of the structure and is given by

$$\boldsymbol{H}(\omega) = \int_{-\infty}^{\infty} \boldsymbol{h}(t)\,\mathrm{e}^{-\mathrm{i}\omega\tau}\,\mathrm{d}\tau \tag{32}$$

The four terms summed to give the right-hand equality of Eq. (31) can be grouped into three parts. These are: the first term corresponds to the contribution of the dynamic component, the second term corresponds the contribution of the quasi-static component and, the sum of the third and the fourth terms represents the contribution of their cross-correlation.

Substituting Eq. (17) into Eq. (31), the power spectrum density matrix of $\boldsymbol{z}(t)$ is expressed by

$$\begin{aligned}\boldsymbol{S}_{zz}(\omega) &= \left(\boldsymbol{T}^{\mathrm{T}}\boldsymbol{H}(\omega)\boldsymbol{A} + \frac{\boldsymbol{G}}{\omega^2}\right)^{*}\boldsymbol{P}^{*}\boldsymbol{P}^{\mathrm{T}}\left(\boldsymbol{T}^{\mathrm{T}}\boldsymbol{H}(\omega)\boldsymbol{A} + \frac{\boldsymbol{G}}{\omega^2}\right)^{\mathrm{T}} \\ &= \boldsymbol{V}^{*}\boldsymbol{V}^{\mathrm{T}}\end{aligned} \tag{33}$$

where

$$\boldsymbol{V} = \left(\boldsymbol{T}^{\mathrm{T}}\boldsymbol{H}(\omega)\boldsymbol{A} + \frac{\boldsymbol{G}}{\omega^2}\right)\boldsymbol{P} \tag{34}$$

On the basis of the PEM, the pseudo-excitation matrix, which can be regarded as N vectors, is constructed as follows:

$$\ddot{\tilde{\boldsymbol{U}}}_b = \boldsymbol{P}\exp(\mathrm{i}\omega t) \tag{35}$$

Then solving the deterministic equations:

$$\boldsymbol{M}\ddot{\tilde{\boldsymbol{U}}}^{\mathrm{d}} + \boldsymbol{C}\dot{\tilde{\boldsymbol{U}}}^{\mathrm{d}} + \boldsymbol{K}\tilde{\boldsymbol{U}}^{\mathrm{d}} = -\boldsymbol{A}\ddot{\tilde{\boldsymbol{U}}}_b \tag{36}$$

gives the pseudo-dynamic displacement matrix $\tilde{\boldsymbol{U}}^{\mathrm{d}}$ as follows:

$$\tilde{\boldsymbol{U}}^{\mathrm{d}} = -\boldsymbol{H}(\omega)\boldsymbol{A}\boldsymbol{P}\exp(\mathrm{i}\omega t) \tag{37}$$

Then, the corresponding pseudo-quasi-static displacement matrix is easily obtained by solving the linear algebraic equations:

$$\boldsymbol{K}\tilde{\boldsymbol{U}}^{s} = \frac{1}{\omega^2}\boldsymbol{K}_{\mathrm{C}}\boldsymbol{E}_{mN}\ddot{\tilde{\boldsymbol{U}}}_b \tag{38}$$

which, by using Eqs. (35) and (21), can be written in the form:

$$\tilde{\boldsymbol{U}}^{s} = -\frac{1}{\omega^2}\boldsymbol{R}\boldsymbol{E}_{mN}\boldsymbol{P}\exp(\mathrm{i}\omega t) \tag{39}$$

and the pseudo-displacement components of support motion along the coordinate axes are given by

$$\tilde{\boldsymbol{U}}_{\mathrm{G}} = -\frac{1}{\omega^2}\boldsymbol{E}_{mN}\boldsymbol{P}\exp(\mathrm{i}\omega t) \tag{40}$$

Therefore, the pseudo-response matrix $\tilde{\boldsymbol{Z}}(t)$ can be expressed as follows:

$$\tilde{\boldsymbol{Z}}(t) = -\left(\boldsymbol{T}^{\mathrm{T}}\boldsymbol{H}(\omega)\boldsymbol{A} + \frac{G}{\omega^2}\right)\boldsymbol{P}\exp(\mathrm{i}\omega t) = -\boldsymbol{V}\exp(\mathrm{i}\omega t) \tag{41}$$

Comparing Eq. (41) with Eqs. (33) and (34), it is not difficult to obtain the relationship:

$$\boldsymbol{S}_{zz}(\omega) = \tilde{\boldsymbol{Z}}^{*}(t)\tilde{\boldsymbol{Z}}^{\mathrm{T}}(t) \tag{42}$$

The required spectral moments of the responses can then be obtained, and so the extreme values can be estimated [37].

The dynamic analysis of complicated structures is usually solved by the mode superposition method, in which $\tilde{\boldsymbol{U}}^{\mathrm{d}}$ in Eq. (36) is expressed in terms of the mode matrix $\boldsymbol{\Phi}$:

$$\tilde{\boldsymbol{U}}^{\mathrm{d}} = \boldsymbol{\Phi}\tilde{\boldsymbol{Y}} \tag{43}$$

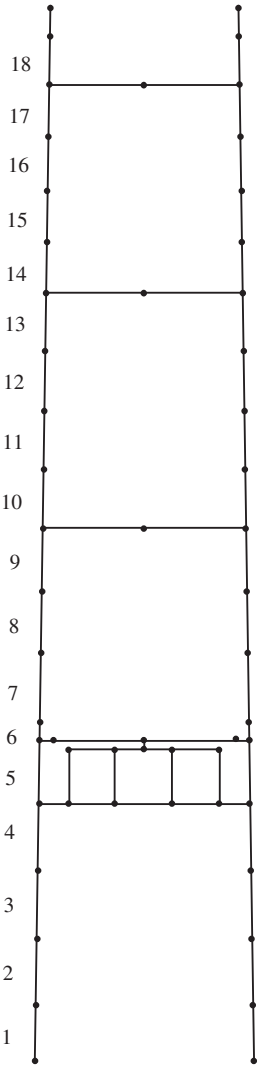

Fig. 4. Some members of the Ma Wan Tower.

where $\boldsymbol{\Phi}$ consists of the first q undamped modes and satisfies:

$$\boldsymbol{K\Phi} = \boldsymbol{M\Phi\Omega}^2 \tag{44}$$

Here $\boldsymbol{\Omega}^2$ is a diagonal matrix consisting of the squares of the first q free vibration frequencies. Using the mass normalized mode matrix, Eq. (36) can be transformed into:

$$\ddot{\tilde{\boldsymbol{Y}}} + \hat{\boldsymbol{C}}\dot{\tilde{\boldsymbol{Y}}} + \boldsymbol{\Omega}^2\tilde{\boldsymbol{Y}} = -\boldsymbol{\Phi}^{\mathrm{T}}\boldsymbol{A}\ddot{\boldsymbol{U}}_b \tag{45}$$

in which

$$\hat{\boldsymbol{C}} = \boldsymbol{\Phi}^{\mathrm{T}}\boldsymbol{C}\boldsymbol{\Phi} \tag{46}$$

If $\boldsymbol{C}$ is an orthogonal damping matrix, $\hat{\boldsymbol{C}}$ will be a diagonal matrix. Then from Eq. (44), it is easily verified that

$$\boldsymbol{\Phi}^{\mathrm{T}}\boldsymbol{MR} = -\boldsymbol{\Omega}^{-2}\boldsymbol{\Phi}^{\mathrm{T}}\boldsymbol{K}\boldsymbol{K}^{-1}\boldsymbol{K}_{\mathrm{C}} = -\boldsymbol{\Omega}^{-2}\boldsymbol{\Phi}^{\mathrm{T}}\boldsymbol{K}_{\mathrm{C}} \tag{47}$$

where $\boldsymbol{\Omega}^{-2}$ is the inverse of $\boldsymbol{\Omega}^2$, which is obtained by replacing the diagonal terms of $\boldsymbol{\Omega}^2$ by their reciprocals, and Eq. (45) can be written as follows:

$$\ddot{\tilde{\boldsymbol{Y}}} + \hat{\boldsymbol{C}}\dot{\tilde{\boldsymbol{Y}}} + \boldsymbol{\Omega}^2\tilde{\boldsymbol{Y}} = (\boldsymbol{\Omega}^{-2}\boldsymbol{\Phi}^{\mathrm{T}}\boldsymbol{K}_{\mathrm{C}} - \boldsymbol{\Phi}^{\mathrm{T}}\boldsymbol{M}_{\mathrm{C}})\boldsymbol{E}_{mN}\ddot{\boldsymbol{U}}_b \tag{48}$$

The above has summarized the key details of PEM associated with multi-support seismic analysis, i.e. the method used to obtain the results which follow.

4. Numerical example

As well as demonstrating applications of the method presented, an example in this section examines the effects of wave passage, incoherence and site–response. The example is an existing bridge structure and shows the powerful potential of the proposed method used, as well as leading to conclusions.

Consider the Tsing-Ma long-span suspension bridge shown in Fig. 1, which links the commercial centers of Hong Kong Island and Kowloon to Hong Kong's airport on Lantau Island. Stretching from Tsing Yi island to Ma Wan island, the Tsing-Ma bridge has a main span of 1377 m between its two towers. The height of the towers is 206 m, the two cables are 36 m apart and the side spans are 300 and 355.5 m, measured to the anchorages. The bridge deck is a hybrid steel structure continuous between the two main anchorages and is supported by suspenders in the main span and one side span, and by three piers on the other side span (Fig. 1). The above facts cause some asymmetry about the midspan of the bridge.

A three-dimensional dynamic finite element model was established for the above bridge after the completion of deck-welding connections [38]. Briefly, three-dimensional Timoshenko beam elements with rigid arms were used to model the two bridge towers. The cables and suspenders were modeled by cable elements and the geometric non-linearity due to the deformation of the cables was allowed for when determining the initial shape of the bridge. Since the sectional properties of the bridge deck rather than structural details affect the natural frequencies and mode shapes of the bridge, the deck in the global dynamic analysis of long-span bridges in commonly represented by a single equivalent beam, or two and three equivalent beams, or equivalent plates, to avoid tremendous computational effort. In consideration of the structural system of the Tsing-Ma Bridge deck, a single equivalent beam was used to model the bridge deck in the global dynamic analysis. Because the size and structural system of the deck vary along the longitudinal axis of the deck, six

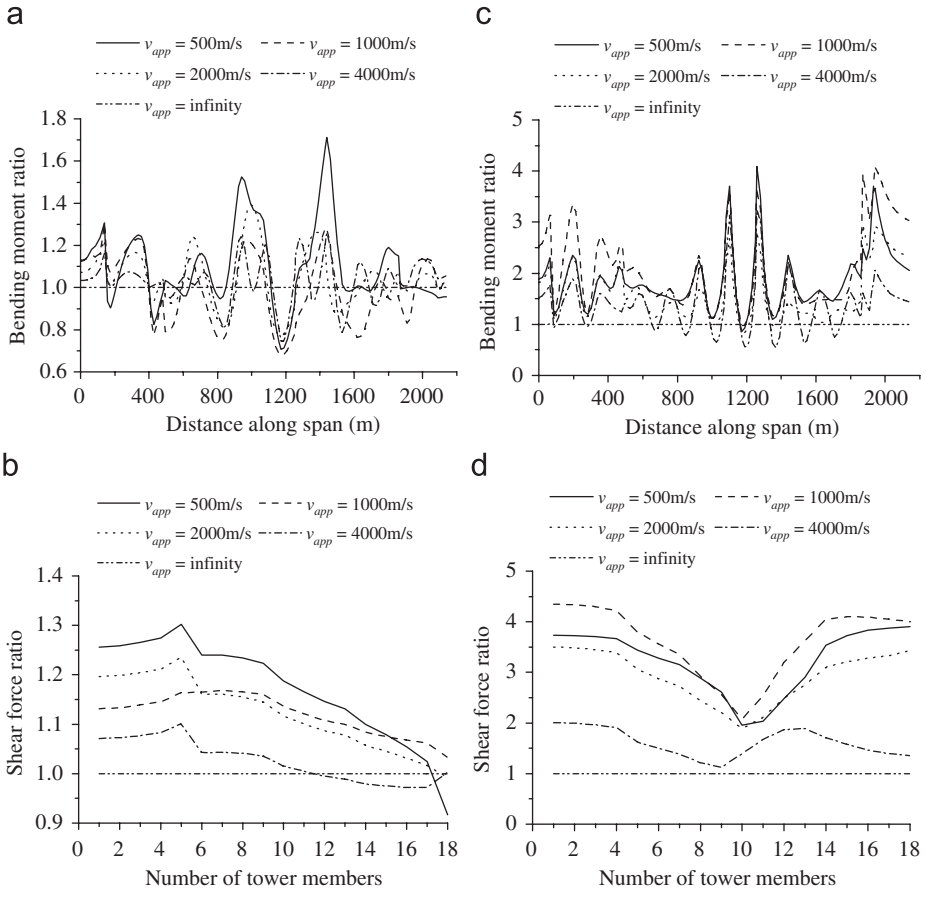

Fig. 5. Ratios of responses relative to the benchmark due to the wave passage effect.

typical cross sections were identified for the whole bridge deck. Each typical section of 18 m was represented by a three-dimensional finite element sectional model generated using the computer program SAP 90. The connections between bridge components and the supports of the bridge were properly modeled. Fig. 2 indicates this finite element model of the Tsing-Ma bridge, which had: 769 nodes, including 29 support ones; 1010 elements and; 2254 degrees of freedom. The proposed method has been implemented on the FEM program DDJ-W. The program can handle three-dimensional Timoshenko beam elements, two-node cable elements, master-slave variables and relative coordinates. The accuracy of the program has been validated through comparison with the results given by some commercial software package in the case of the free-standing towers and equivalent bridge beam, and given by Irvine's theory in the case of the main span and side span cables [38]. The distribution of its first 200 natural frequencies is indicated in Table 1. It can be seen that the natural frequencies of the bridge are very closely spaced. Detailed information on the structural properties, on the finite element modeling, on the natural frequencies and, on the mode shapes of the bridge are given in Ref. [38].

The first 180 modes were used in the mode superposition analysis, because using more modes was shown to make practically no difference. The damping ratios of all participant modes were assumed to be 0.02. The seismic spatial effects for horizontal SH waves and vertical SV waves traveling in the longitudinal direction of the bridge were investigated. The effective frequency region was taken as $\omega \in [0, 15]$ rad/s and the frequency step-size as $\Delta\omega = 0.01$ rad/s. Using a smaller frequency step-size and a wider frequency region was found to make practically no difference to the results.

In the computation that follows, sites with different soil conditions have been modeled using the modified Kanai–Tajimi spectral density function for ground accelerations, $S_{kk}(\omega)$, $k = 1, 2, \ldots, N$, is given by [36]

$$S_{kk}(\omega) = \frac{1 + 4\xi_{gk}^2(\omega/\omega_{gk})^2}{[1 - (\omega/\omega_{gk})^2]^2 + 4\xi_{gk}^2(\omega/\omega_{gk})^2} \times \frac{(\omega/\omega_{fk})^4}{[1 - (\omega/\omega_{fk})^2]^2 + 4\xi_{fk}^2(\omega/\omega_{fk})^2} S_{0k} \tag{49}$$

in which, S_{0k} is the amplitude of the white-noise bedrock acceleration, ω_{gk} and ξ_{gk} are the resonant frequency and damping ratio of the first filter, and ω_{fk} and ξ_{fk} are those of the second filter. In this study, firm, medium and soft soil types are considered and the filter parameters used for these soil types are those proposed by Der Kiureghian and Neuenhofer [15] (Table 2). The values of S_0 were obtained for each soil category by equating the variance of the east–west component of the Erzincan earthquake acceleration record in 1992 [25] and are also listed in Table 2.

Two models are adopted to account for the incoherence effect:

(1) The L–Y model, i.e. the coherency relationship between two arbitrary ground joints was expressed as follows [35]:

$$\gamma_{kl}^{(i)}(\omega) = \exp\left[-\alpha \frac{\omega d_{kl}}{2\pi v_{\text{app}}}\right] \tag{50}$$

where the constant α used was 0.125.

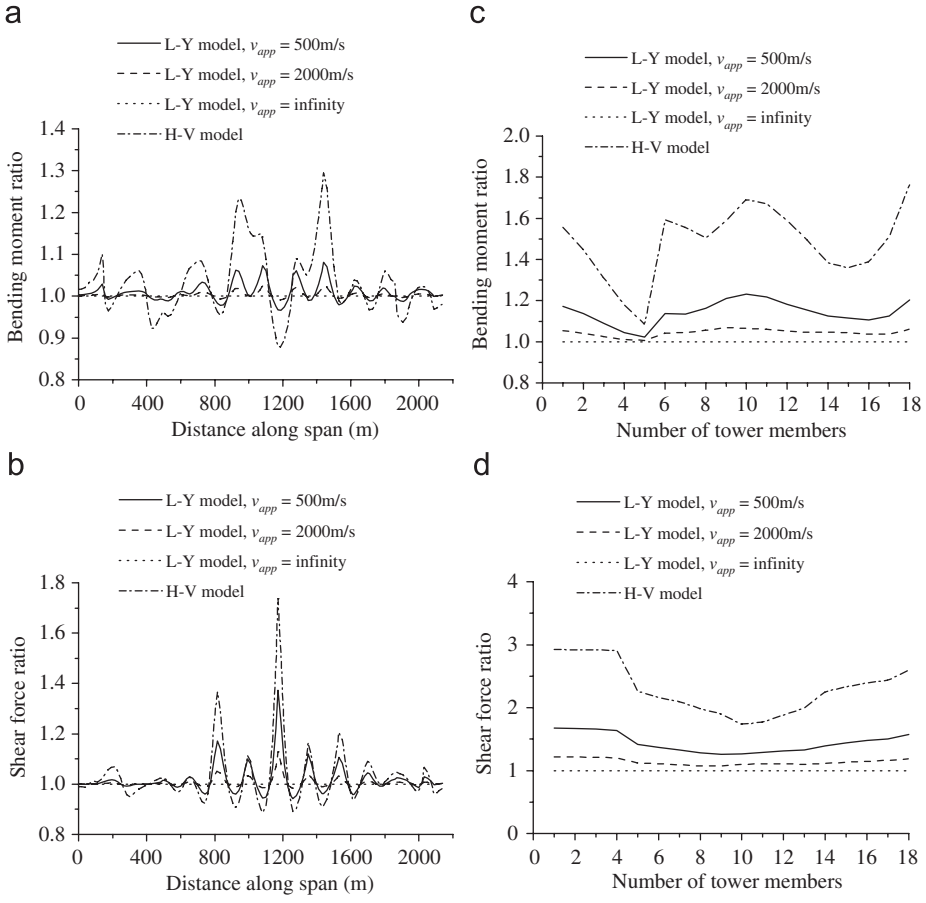

Fig. 6. Ratios of responses relative to the benchmark due to the incoherence effect.

(2) The H–V model, i.e. the coherency relationship was expressed as follows [34]:

$$\gamma_{kl}^{(i)}(\omega) = A\exp\left[-\frac{2d_{kl}}{\alpha\theta(\omega)}(1-A+\alpha A)\right] + (1-A)\exp\left[-\frac{2d_{kl}}{\theta(\omega)}(1-A+\alpha A)\right] \quad (51)$$

in which

$$\theta(\omega) = K[1+(\omega/\omega_0)^b]^{-(1/2)} \quad (52)$$

and the values used for the parameters in Eqs. (51) and (52) were: $A=0.736$, $\alpha=0.147$, $K=5210$, $\omega_0=6.85$ rad/s and, $b=2.78$.

As a benchmark for the comparison, analysis is first carried out using uniform support motions all described by the set of surface motions of the "firm" site. This is referred to the uniform support motion case. The results are illustrated in Fig. 3. Fig. 3(a) presents the transverse shear forces and bending moments in z-direction of the deck under SH waves; Fig. 3(b) shows the transverse shear forces and bending moments in x-direction of some members of the Ma Wan Tower (Fig. 4) under SH waves; Fig. 3(c) gives the vertical shear forces and bending moments in y-direction of the deck under SV waves; and Fig. 3(d) presents the shear forces in x-direction and bending moments in y-direction of some members of the Ma Wan Tower under SV waves.

Fig. 5 presents the ratios of responses relative to the benchmark for a case where spatial variability due to the wave passage effect alone is considered. The wave velocities were as shown, namely 500, 1000, 2000, 4000 m/s and infinity. It can be seen from these figures that many of the ratios are greater than 1. Obviously, the wave passage effect has significant influence on the seismic responses. It is also observed that the influence of wave passage effect on the response of the bridge is not necessarily monotonic.

Fig. 6 shows the ratios of responses relative to the benchmark for a case where spatial variability due to the incoherence effect alone is considered. Four cases are shown: (1) L–Y model, $v_{app}=500$ m/s; (2) L–Y model, $v_{app}=2000$ m/s; (3) L–Y model, $v_{app}=\infty$ and (4) H–V model. It can be observed that the incoherence has significant influence on the seismic responses and that there are notable differences in the results given by the different incoherence models.

To show the influence of the site–response effect, six cases were considered for the soil conditions at Ma Wan and Tsing Yi islands. They were: firm–firm, medium–medium, soft–soft, firm–medium, firm–soft and medium–soft. Fig. 7 presents the results of this analysis. It can be seen that the seismic responses under different soil conditions, i.e. including site-response effect, have significant differences from those under uniform soil conditions. Moreover, these responses are almost always between those of the firmer uniform soil condition and the softer uniform soil condition.

Fig. 8 compares the results for the benchmark case with four cases: (1) the wave passage effect alone, (2) the effects of wave passage and incoherence (L–Y model), (3) the effects of wave passage and incoherence (H–V model) and, (4) the effects of wave passage, incoherence and site–response are all present. In all cases, $v_{app}=1000$ m/s. The support conditions were the same as those of the benchmark case for Cases (1)–(3). In Case (4), the soil condition at Ma Wan and Tsing Yi islands was firm–medium. It can be seen from these figures that variable site conditions of

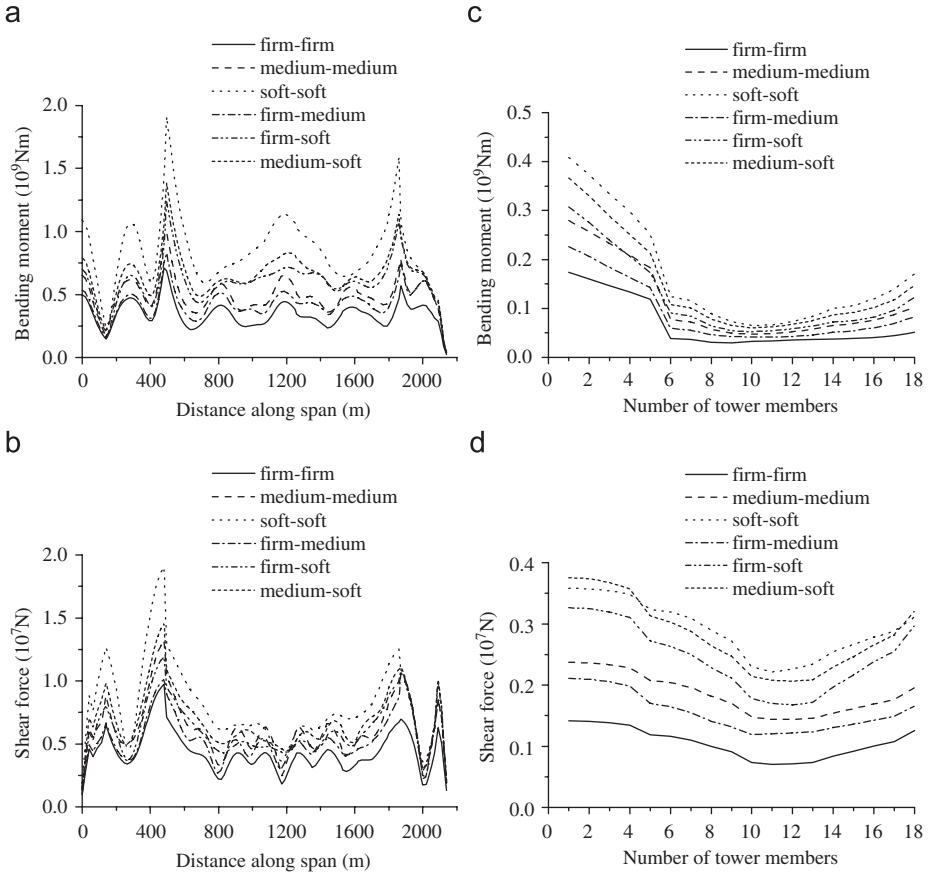

Fig. 7. Responses due to the site–response effect.

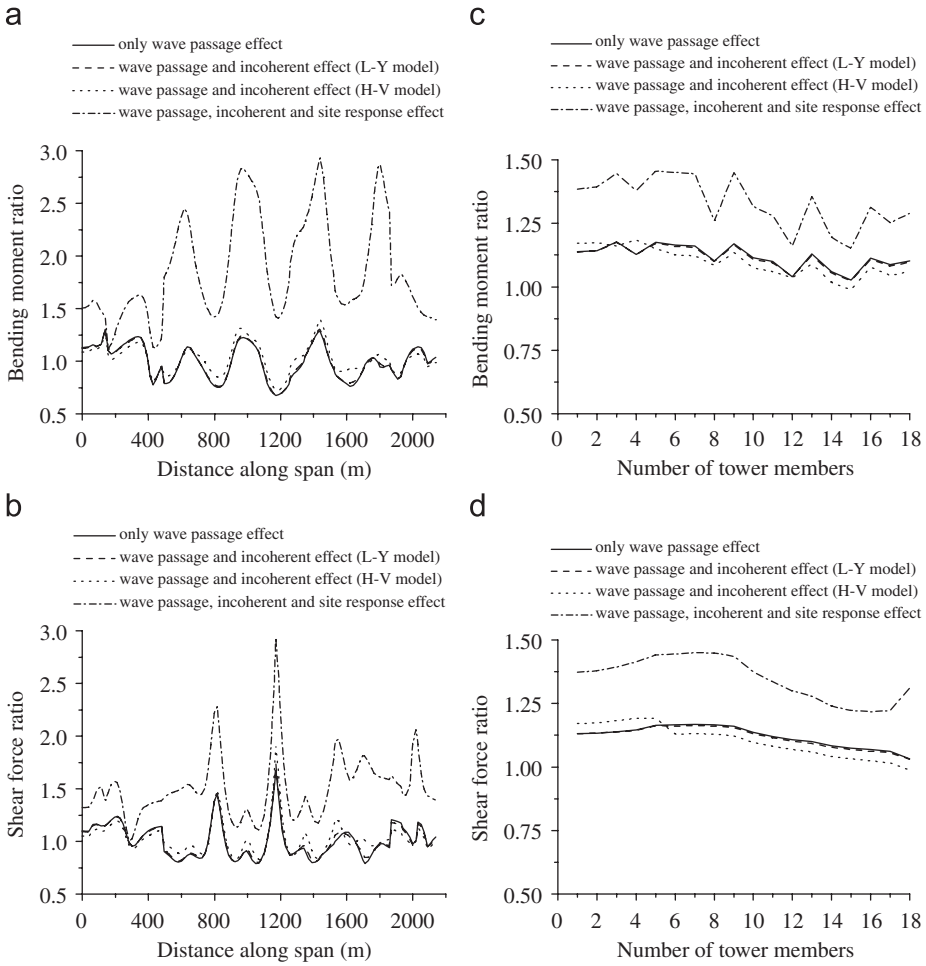

Fig. 8. Ratios of responses relative to the benchmark due to the wave passage, incoherent and site–response effects.

the soil condition at Ma Wan Tower changing from firm to medium, had larger effects on the shear forces and bending moments of the bridge than others.

5. Conclusions

This paper presents a random vibration algorithm for the seismic–response analysis which accurately accounts for the spatial variability effects of wave passage, incoherence and site–response.

Complex structures usually have very closely spaced natural frequencies and it is difficult to judge which of these will affect the structural responses severely. It is difficult to make general conclusions for this complex problem. The results presented for a suspension bridge show that the response depends heavily on the three spatial variability effects. Therefore, for realistic seismic analysis of long-span structures the variability of the ground motions should be incorporated.

Acknowledgments

The authors are grateful for support under grants from the City University of Hong Kong (Project no. 7001591), from NSFC (No. 10502011) and from the Cardiff University Advanced Chinese Engineering Centre.

References

[1] Zerva A, Zervas V. Spatial variation of seismic ground motions: an overview. Appl Mech Rev 2002;55(3):271–97.
[2] Der Kiureghian A. A coherency model for spatially varying ground motions. Earthquake Eng Struct Dyn 1996;25(1):99–111.
[3] Lee MC, Penzien J. Stochastic analysis of structures and piping systems subjected to stationary multiple support excitations. Earthquake Eng Struct Dyn 1983;11(1):91–110.
[4] Lin YK, Zhang R, Yong Y. Multiply supported pipeline under seismic wave excitations. J Eng Mech ASCE 1990;116(5):1094–108.
[5] Perotti F. Structural response to non-stationary multiple-support random excitation. Earthquake Eng Struct Dyn 1990;19(4):513–27.
[6] Loh CH, Lee SZ. Aseismic displacement analysis of multi-supported bridge to multiple excitations. Soil Dyn Earthquake Eng 1990;9(1):25–33.
[7] Yamamura N, Tanaka H. Response analysis of flexible MDF systems for multiple-support seismic excitations. Earthquake Eng Struct Dyn 1990;19(3):345–57.
[8] Deodatis G, Saxena V, Shinozuka M. Effect of spatial variability of ground motion on bridge fragility curves. In: Proceedings of the eighth specialty conference on probabilistic mechanics and structural reliability 2000. PMC2000-125. University of Notre Dame, Indiana.
[9] Zerva A. Response of multi-span beams to spatially incoherent seismic ground motions. Earthquake Eng Struct Dyn 1990;19(6):819–32.
[10] Zerva A. Effect of spatial variability and propagation of seismic ground motions on the response of multiply supported structures. Probab Eng Mech 1991;6(3-4):212–21.
[11] Zerva A. Seismic loads predicted by spatial variability models. Struct Safety 1992;11(3–4):227–43.
[12] Zerva A. On the spatial vibration of seismic ground motions and its effects on lifelines. Eng Struct 1994;16(1):534–46.
[13] Berrah M, Kausel E. A modal combination rule for spatially varying seismic motions. Earthquake Eng Struct Dyn 1993;22(9):791–800.
[14] Nazmy AS, Abdel-Ghaffar AM. Effects of ground motion spatial variability on the response of cable-stayed bridges. Earthquake Eng Struct Dyn 1992;21(1):1–20.

[15] Der Kiureghian A, Neuenhofer A. Response spectrum method for multi-support seismic excitations. Earthquake Eng Struct Dyn 1992;21(8):713–40.
[16] Heredia-Zavoni E, Vanmarcke EH. Seismic random vibration analysis of multi-support structural systems. J Eng Mech ASCE 1994;120(5):1107–28.
[17] Harichandran RS, Wang W. Response of simple beam to spatially varying earthquake excitation. J Eng Div, ASCE 1988;114(9):1526–41.
[18] Harichandran RS, Wang W. Response of indeterminate two-span beam to spatially varying earthquake excitation. Earthquake Eng Struct Dyn 1990; 19(2):173–87.
[19] Harichandran RS. An efficient, adaptive algorithm for large scales random vibration analysis. Earthquake Eng Struct Dyn 1993;22(2):151–65.
[20] Harichandran RS, Hawwari A, Sweidan BN. Response of long-span bridges to spatially varying ground motion. J Struct Eng, ASCE 1996;122(5):476–84.
[21] Tubino F, Carassale L, Solari G. Seismic response of multi-supported structures by proper orthogonal decomposition. Earthquake Eng Struct Dyn 2003;32(11):1639–54.
[22] Allam SM, Datta TK. Seismic behaviour of cable-stayed bridges under multi-component random ground motion. Eng Struct 1999;21(1):62–74.
[23] Allam SM, Datta TK. Analysis of cable-stayed bridges under multi-component random ground motion by response spectrum method. Eng Struct 2000; 22(10):1367–77.
[24] Zanardo G, Hao H, Modena C. Seismic response of multi-span simply supported bridges to a spatially varying earthquake ground motion. Earthquake Eng Struct Dyn 2002;31(6):1325–45.
[25] Dumanoglu AA, Soyluk K. A stochastic analysis of long span structures subjected to spatially varying ground motions including the site-response effect. Eng Struct 2003;25(10):1301–10.
[26] Soyluk K, Dumanoglu AA. Spatial variability effects of ground motions on cable-stayed bridges. Soil Dyn Earthquake Eng 2004;24(3):241–50.
[27] Adanur S, Soyluk K, Bayraktar A, Dumanoglu AA. Stochastic seismic response of the bosporus suspension bridge to spatially varying ground motions. In: Proceedings of the first European conference on earthquake engineering and seismology, 1st ECEES, 3–8 September 2006, Geneva, Switzerland. p. 300.
[28] Lupoi A, Franchin P, Pinto P E, Monti G. Seismic design of bridges accounting for spatial variability of ground motion. Earthquake Eng Struct Dyn 2005;34(4–5):327–48.
[29] Lin JH. A fast CQC algorithm of PSD matrices for random seismic responses. Comput Struct 1992;44(3):683–7.
[30] Lin JH, Li JJ, Zhang WS, Williams FW. Non-stationary random seismic responses of multi-support structures in evolutionary inhomogeneous random fields. Earthquake Eng Struct Dyn 1997;26(1):135–45.
[31] Lin JH, Zhang YH, Li QS, Williams FW. Seismic spatial effects for long-span bridges, using the pseudo-excitation method. Eng Struct 2004;26(9):1207–16.
[32] Zhang YH, Lin JH, Williams FW, Li QS. Wave passage effect of seismic ground motions on the response of multiply supported structures. Struct Eng Mech 2005;20(6):655–72.
[33] Luco JE, Wong HL. Response of a foundation to a spatially random ground motion. Earthquake Eng Struct Dyn 1986;14(6):891–908.
[34] Harichandran RS, Vanmarcke EH. Stochastic variation of earthquake ground motion in space and time. J Eng Mech ASCE 1986;112(2):154–75.
[35] Loh CH, Yeh YT. Spatial variation and stochastic modeling of seismic differential ground movement. Earthquake Eng Struct Dyn 1988;16(5): 583–96.
[36] Clough RW, Penzien J. Dynamics of structures. New York: McGraw-Hill; 1993.
[37] Davenport AG. The application of statistical concepts to the wind loading of structures. Proc Inst Civil Eng 1961;19:449–72.
[38] Xu YL, Ko JM, Zhang WS. Vibration studies of Tsing Ma suspension bridge. J Bridge Eng ASCE 1997;2(4):149–56.